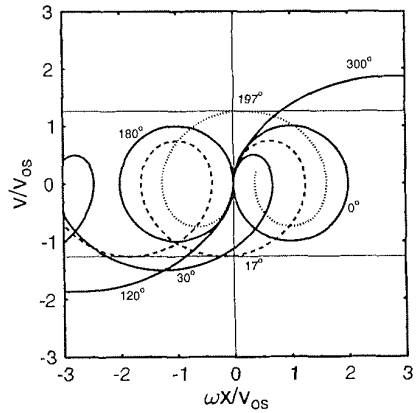

Fig. 2.5 Phase-space portrayal of recollision model. The orbits all start at the origin $(0,0)$ and proceed clockwise. The maximum velocity at the recrossing point $x = 0$ is indicated by the horizontal limits at $v_m/v_{os} = \pm\sqrt{3.17/2}$.

pump beam, which in turn can limit the efficiency of the harmonics (Balcou and L'Huillier, 1993; Tisch *et al.*, 1994).

The experimental pursuit of high harmonics from gas targets has concentrated on finding ways to extend the plateau region, thereby producing harmonics with ever smaller wavelengths. The obvious option of increasing the laser intensity — and thus U_p — only works up to a certain *saturation intensity*, beyond which most of the harmonic-producing atoms become ionized. Ions themselves (for example He^+) are also candidates for HHG by virtue of their higher ionization potential I_p, and have been investigated experimentally (Preston *et al.*, 1996). The most promising route to date, however, is to use extremely short (few-cycle) pulses, which appears to enable atoms to survive a bit longer at higher intensities, extending the range of observed harmonics well beyond the $I_p + 3U_p$ limit (Zhou *et al.*, 1996; Christov *et al.*, 1997; Schnürer *et al.*, 1998).

Chapter 3

Interaction with Single Electrons

3.1 Motion of an Electron in an Electromagnetic Plane Wave

The starting point for many early investigations on nonlinear laser-matter interaction was the orbit of a single electron in a strong electromagnetic plane-wave. This well-known problem can be solved exactly (Landau and Lifshitz, 1962; Gunn and Ostriker, 1971; Eberly and Sleeper, 1968), and is conveniently described in terms of an 'average rest frame', which drifts with a particular velocity with respect to the laboratory frame (the magnitude of which will be derived shortly). Although this ground has been well covered in the literature, and is frequently revisited (Bardsley *et al.*, 1989; Hartemann, 1998; San Roman *et al.*, 2000), it will prove worthwhile to review the main results in order to introduce some notation, and also to get a feel for the nonlinear electron dynamics which lies behind the more complex laser-plasma interactions which we will come to in the Chapters 4 and 5.

The motion of a particle in the presence of electromagnetic fields $\boldsymbol{E}$ and $\boldsymbol{B}$ wave is described by the Lorentz equation,

$$\frac{d\boldsymbol{p}}{dt} = -e(\boldsymbol{E} + \frac{1}{c}\boldsymbol{v} \times \boldsymbol{B}), \tag{3.1}$$

together with an energy equation

$$\frac{d}{dt}\left(\gamma mc^2\right) = -e(\boldsymbol{v} \cdot \boldsymbol{E}), \tag{3.2}$$

where $\boldsymbol{p} = \gamma m\boldsymbol{v}$, and $\gamma = (1 + p^2/m^2c^2)^{\frac{1}{2}}$ is the relativistic factor.

An elliptically polarized plane-wave $\boldsymbol{A}(\omega, \boldsymbol{k})$ traveling in the positive

x-direction can be represented by the wave vector

$$\boldsymbol{A} = (0, \delta a_0 \cos\phi, (1-\delta^2)^{\frac{1}{2}} a_0 \sin\phi), \tag{3.3}$$

where $\phi = \omega t - kx$ is the phase of the wave; a_0 is the normalized amplitude (v_{os}/c), and δ is a *polarization* parameter such that $\delta = \{\pm 1, 0\}$ for a linearly polarized wave and $\pm 1/\sqrt{2}$ for a circular wave. To simplify the working, we now introduce the normalizations: $t \to \omega t, x \to kx, \boldsymbol{v} \to \boldsymbol{v}/c, \boldsymbol{p} \to \boldsymbol{p}/mc$, and $\boldsymbol{A} \to e\boldsymbol{A}/mc^2$. (This is equivalent to setting $\omega = k = c = e = m = 1$, as with the atomic units in the previous chapter.) Using the relations $\boldsymbol{E} = -\partial\boldsymbol{A}/\partial t$ and $\boldsymbol{B} = \nabla \times \boldsymbol{A} = (0, -\partial A_z/\partial x, \partial A_y/\partial x)$, the perpendicular component of Eq. (3.1) becomes:

$$\frac{d\boldsymbol{p}_\perp}{dt} = \frac{\partial \boldsymbol{A}}{\partial t} + v_x \frac{\partial \boldsymbol{A}}{\partial x},$$

which after integrating gives:

$$\boldsymbol{p}_\perp - \boldsymbol{A} = \boldsymbol{p}_{\perp 0}, \tag{3.4}$$

where $\boldsymbol{p}_{\perp 0}$ is a constant of motion representing the initial perpendicular momentum of the electron. This might be non-zero if the electron had just been ejected from an atom via multiphoton ionization, say. The longitudinal components of Eq. (3.1) and Eq. (3.2) yield a pair of equations which can be subtracted from each other thus:

$$\frac{dp_x}{dt} - \frac{d\gamma}{dt} = -v_y\left(\frac{\partial A_y}{\partial t} + \frac{\partial A_y}{\partial x}\right) - v_z\left(\frac{\partial A_z}{\partial t} + \frac{\partial A_z}{\partial x}\right).$$

Because the EM wave is a function of $t - x$ only, the terms on the RHS vanish identically, so we can immediately integrate the RHS to get:

$$\gamma - p_x = \alpha,$$

where α is a constant of motion still to be determined. Using the identity $\gamma^2 - p_x^2 - p_\perp^2 = 1$ and choosing $\boldsymbol{p}_{\perp 0} = 0$, we can eliminate γ to get a relationship between the parallel and perpendicular momenta:

$$p_x = \frac{1 - \alpha^2 + p_\perp^2}{2\alpha}. \tag{3.5}$$

Since Eq. (3.4) now tells us that $p_\perp$ is equal to the laser vector potential, Eq. (3.5) represents the general (Lorentz-covariant) solution for the motion of free electrons in an electromagnetic wave (Bardsley *et al.*, 1989). To

proceed, we need to specify α and integrate Eq. (3.4) and Eq. (3.5). The latter is simplified by changing variables. Noting that

$$\frac{d\phi}{dt} = \frac{\partial\phi}{\partial t} + \frac{p_x}{\gamma}\frac{\partial\phi}{\partial x} = \frac{\alpha}{\gamma},$$

we have

$$\boldsymbol{p} = \gamma\frac{d\boldsymbol{r}}{dt} = \gamma\frac{d\phi}{dt}\frac{d\boldsymbol{r}}{d\phi} = \alpha\frac{d\boldsymbol{r}}{d\phi}. \tag{3.6}$$

3.1.1 *Laboratory frame*

In the laboratory frame, the electron is initially at rest before the EM wave arrives, so that at $t = 0$, $p_x = p_y = 0$ and $\gamma = 1$. From the conservation relation Eq. (3.5) it follows that $\alpha = 1$ in this case. This leads to the following expression for the momenta in the lab frame:

$$\begin{aligned} p_x &= \frac{a_0^2}{4}\left[1 + (2\delta^2 - 1)\cos 2\phi\right], \\ p_y &= \delta a_0 \cos\phi, \\ p_z &= (1-\delta^2)^{1/2} a_0 \sin\phi. \end{aligned} \tag{3.7}$$

With the help of Eq. (3.6) we can integrate expressions Eqs. (3.7a–3.7c) to obtain the lab-frame orbits valid for arbitrary polarization δ:

$$\begin{aligned} x &= \frac{1}{4}a_0^2\left[\phi + \frac{2\delta^2 - 1}{2}\sin 2\phi\right], \\ y &= \delta a_0 \sin\phi, \\ z &= -(1-\delta^2)^{1/2} a_0 \cos\phi. \end{aligned} \tag{3.8}$$

This solution, which exhibits a self-similarity in the variables $(x/a_0^2, y/a_0)$, is shown graphically in Fig. 3.1. We notice immediately that regardless of polarization, the longitudinal motion has a secular component which will grow in time or with propagation distance. In fact, in the presence of the EM wave, the electron immediately starts to *drift* with an average momentum $p_D \equiv \overline{p_x} = a_0^2/4$, corresponding to a velocity (see also Exercise 2 on p. 52):

$$\frac{v_D}{c} = \overline{v_x} = \frac{\overline{p_x}}{\overline{\gamma}} = \frac{a_0^2}{4 + a_0^2}, \tag{3.9}$$

where the overscore denotes averaging over the rapidly varying EM phase ϕ.

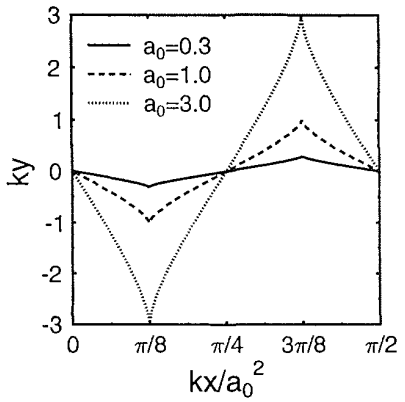

Fig. 3.1 Electron orbits in a large amplitude, linearly polarized electromagnetic plane wave. For a 1 μm laser wavelength, the pump strengths a_0 correspond roughly to intensities of 10^{17}, 10^{18} and 10^{19} Wcm^{-2} respectively.

For circularly polarized light ($\delta = \pm 1/\sqrt{2}$), the longitudinal oscillating component at 2ϕ vanishes identically, and the transverse motion is circular with radius a_0 and momentum $p_\perp = a_0/\sqrt{2}$. This combines with the linear drift in Eq. (3.9) to give a *helical* orbit with pitch angle

$$\theta_p = p_\perp/p_D = \sqrt{8}a_0^{-1}. \tag{3.10}$$

3.1.2 *Average rest frame*

The fact that the electron drifts in the lab-frame leads naturally to another possible choice of constant α. If we instead require that this drift velocity vanish for arbitrary pump strengths, then we set $\overline{p_x} = 0$ in Eq. (3.5) to get:

$$1 + \overline{A^2} - \alpha^2 = 0.$$

Averaging over a laser cycle to remove rapidly varying terms, and noting that $\overline{\cos^2\phi} = 1/2$ gives:

$$\alpha = \left(1 + \frac{a_0^2}{2}\right)^{1/2} \equiv \gamma_0. \tag{3.11}$$

Plugging this back into Eq. (3.5) gives the momenta:

$$p_x = \left(2\delta^2 - 1\right)\frac{a_0^2}{4\gamma_0}\cos 2\phi, \tag{3.12}$$

$$p_y = \delta a_0 \cos\phi,$$

$$p_z = (1-\delta^2)^{\frac{1}{2}} a_0 \sin\phi. \tag{3.13}$$

Noting that in this case, $\boldsymbol{p} = \gamma_0 d\boldsymbol{r}/d\phi$, we can integrate again to get the orbits:

$$x = \left(\delta^2 - \frac{1}{2}\right) q^2 \sin 2\phi,$$

$$\boldsymbol{r}_\perp = 2(\delta q \sin\phi, -(1-\delta^2)^{\frac{1}{2}} q \cos\phi), \tag{3.14}$$

where $q = a_0/2\gamma_0$. Eliminating ϕ for linear polarization ($\delta = 1$), we obtain the famous *figure-of-eight* shown in Fig. 3.2.

$$16x^2 = y^2(4q^2 - y^2). \tag{3.15}$$

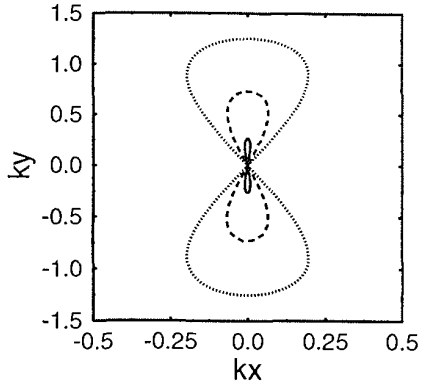

Fig. 3.2 Characteristic orbits of free electrons in a plane electromagnetic wave in the average rest frame. The trajectories correspond to the same light intensities as in Fig. 3.1.

In the extreme intensity limit, $a_0 \gg 1$, we find $\gamma_0 \to a_0/\sqrt{2}$ and $q \to 1/\sqrt{2}$, so that the orbit becomes a 'fat-8' with proportions $|\ x\ |_{\max} = 1/4$,

$y\,|_{\max} = \sqrt{2}$. Note that the laboratory frame orbits described by Eq. (3.8) can also be obtained by back-transformation of Eq. (3.14), see Exercise 2c. For circularly polarized light ($\delta = \pm 1/\sqrt{2}$), the longitudinal component vanishes identically, and the electron simply describes a circle with radius $a_0/\sqrt{2}\gamma_0$.

3.1.3 *Finite pulse duration*

The exact analytical solutions for plane waves are of course useful to have, but do not completely describe the details of electron motion caused by a real laser pulse. We can generalize these results to some extent by imposing a *temporal envelope* on the wave vector of the form:

$$A(x,t) = a_0 f(t) \cos\phi, \tag{3.16}$$

where $f(t)$ is considered to be slowly varying relative to the laser cycle: $df/dt \ll \omega f$. In this adiabatic approximation, we can directly substitute $a_0 f(t)$ for a_0 in the solutions given by Eqs. (3.7,3.8). Alternatively, the finite-difference form of Eq. (4.1) can be integrated directly, see Sec. 6.4. As an example, consider the motion caused by a '$\sin^2$' pulse: $f(t) = \sin(\pi t/2t_L)$ with duration $\omega t_L = 600/\pi$. The resulting electron orbit (computed here numerically) in Fig. 3.3 verifies two of the important points made above: namely, that the transverse momentum is conserved: $p_y(t) = A_y(t)$, and that the electron returns to rest after the laser has passed.

3.2 Ponderomotive Force

The solutions derived in the previous section are, strictly speaking, only valid for plane waves; radiation whose magnitude is uniform in space and slowly varying in time. Short pulse lasers of course tend to violate this condition on all fronts: tight focusing creates strong radial intensity gradients over a few wavelengths; ultrashort, few-cycle pulses are highly dispersive and demand a completely non-adiabatic treatment. For the time-being, the emphasis will be on the first of these cases: the cigar-shaped pulses typical of laser systems producing pulses with durations in excess of 50 fs.

There are few topics in laser-plasma interactions that have caused such persistent argument and controversy as the curiously named *ponderomotive force*. On a purely heuristic level, it is relatively straightforward to

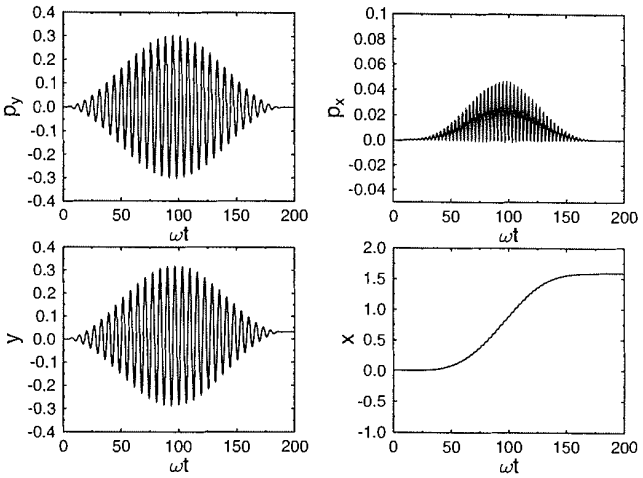

Fig. 3.3 Electron orbit generated by a finite-duration laser pulse.

define: namely as the gradient of the time-averaged 'oscillation potential' introduced in the previous chapter. Historically, problems have arisen when attempting to reconcile the single-particle definition with a more general plasma fluid picture (Hora, 1981). More recently, attention has turned to the relativistic version of this effect — an effort which has acquired poignancy now that high-intensity lasers have made direct tests of theory possible.

Rather than attempt a rigorous derivation here, I will stick to heuristic arguments in order to gain an intuitive feel for ponderomotive behavior. First consider the non-relativistic case of a single electron oscillating near the center of a focused laser beam, see Fig. 3.4. In the limit $v/c \ll 1$, the equation of motion (3.1) for the electron becomes:

$$\frac{\partial v_y}{\partial t} = -\frac{e}{m} E_y(\boldsymbol{r}). \tag{3.17}$$

The EM wave is taken to be propagating in the +ve x-direction as before, but this time with a radial intensity dependence, which for the time-being we will assume to be in the y-direction only. Taylor expansion of the electric

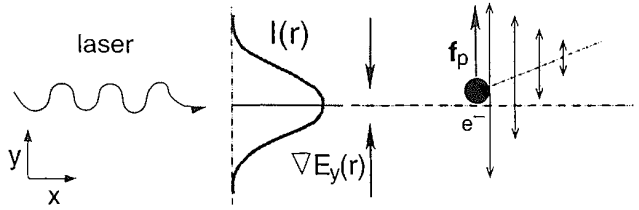

Fig. 3.4 Schematic view of the radial ponderomotive force due to a focused beam.

field then gives:

$$E_y(r) \simeq E_0(y)\cos\phi + y\frac{\partial E_0(y)}{\partial y}\cos\phi + ...,$$

where $\phi = \omega t - kx$ as before. To lowest order, we therefore have

$$v_y^{(1)} = -v_{os}\sin\phi; \quad y^{(1)} = \frac{v_{os}}{\omega}\cos\phi,$$

where v_{os} is defined as usual by Eq. (2.19). Substituting back into Eq. (3.17) gives

$$\frac{\partial v_y^{(2)}}{\partial t} = -\frac{e^2}{m^2\omega^2}E_0\frac{\partial E_0(y)}{\partial y}\cos^2\phi.$$

Multiplying by m and taking the cycle-average yields the ponderomotive force on the electron:

$$f_p \equiv m\overline{\frac{\partial v_y^{(2)}}{\partial t}} = -\frac{e^2}{4m\omega^2}\frac{\partial E_0^2}{\partial y}. \tag{3.18}$$

We see immediately that this expression is just the (-ve) gradient of the ponderomotive potential Eq. (2.6) introduced in Chapter 2. Physically, the force will tend to push electrons away from regions of locally higher intensity. A single electron will therefore inevitably drift away from the center of focused laser beam, picking up a velocity $v \sim v_{os}$ in the process. This conversion of oscillatory to directed energy will be analyzed shortly, but first consider the fully relativistic version of Eq. (3.18). Rewriting our original Lorentz equation (3.1) in terms of the vector potential $\boldsymbol{A}$, we have:

$$\frac{\partial \boldsymbol{p}}{\partial t} + (\boldsymbol{v}.\nabla)\boldsymbol{p} = \frac{e}{c}\frac{\partial \boldsymbol{A}}{\partial t} - \frac{e}{c}\boldsymbol{v}\times\nabla\times\boldsymbol{A}. \tag{3.19}$$

To progress further, we separate the timescales of the electron motion into slow and fast components: $\boldsymbol{p} = \boldsymbol{p}^s + \boldsymbol{p}^f$, and use the following identity:

$$\begin{aligned}\boldsymbol{v}\times(\nabla\times\boldsymbol{p}) &= \frac{1}{m\gamma}\boldsymbol{p}\times\nabla\times\boldsymbol{p} \\ &= \frac{1}{2m\gamma}\nabla \mid p \mid^2 - \frac{1}{m\gamma}(\boldsymbol{p}.\nabla)\boldsymbol{p}.\end{aligned}$$

To lowest order, the fast (transverse) component of the electron momentum follows the vector potential: $\boldsymbol{p}^f = e\boldsymbol{A}/c$ as before. Averaging over a laser cycle, we arrive at the following expression for the relativistic ponderomotive force:

$$\boldsymbol{f}_p = \frac{d\boldsymbol{p}^s}{dt} = -mc^2\nabla\overline{\gamma}, \tag{3.20}$$

where $\gamma = (1 + p_s^2/m^2c^2 + a_0^2/2)^{1/2}$. This derivation is far from rigorous, but the result is actually equivalent to more sophisticated analyses using covariant (Startsev and McKinstrie, 1997) or Lagrangian (Bauer *et al.*, 1995) formulations.

3.3 Ejection from Focused Laser Beam

Solving the electron motion via Eq. (3.20) for a general laser intensity profile is only possible numerically, since the ponderomotive force is a nonlinear function of the electron's momentum and position. What we *can* do analytically is to determine the electron's final state, i.e. its momenta after having been ejected from the beam focus. We have already seen that in the low-intensity (non-relativistic) case, the electron will simply be accelerated out of the focal region at 90^o to the laser axis. At higher intensities, the relativistic drift motion starts to kick in, causing the electron to be directed forwards as well as sideways, see Fig. 3.5. To determine the ejection angle θ, we do some simple relativistic kinematics. We first observe that the final kinetic energy of the electron is just given by:

$$\Delta U = (\gamma - 1)mc^2. \tag{3.21}$$

This energy is extracted from the electromagnetic field via multiphoton momentum transfer. Since the parallel momentum is conserved, we must have:

$$p_\parallel = n\hbar k = \frac{n\hbar\omega}{c} = \frac{\Delta U}{c} = (\gamma - 1)mc. \tag{3.22}$$

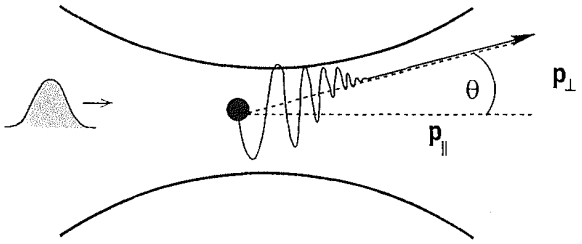

Fig. 3.5 Relativistic electron motion in extended laser focus.

Recalling the relationship from Eq. (3.5) between $p_\parallel$ and $p_\perp$ found earlier (with $\alpha = 1$), we have

$$p_\parallel = \frac{p_\perp^2}{2mc},$$

so the emission angle is given simply by:

$$\tan\theta = \frac{p_\perp}{p_\parallel} = \sqrt{\frac{2}{\gamma - 1}}, \tag{3.23}$$

or

$$\cos\theta = \sqrt{\frac{\gamma - 1}{\gamma + 1}}.$$

This surprisingly simple one-to-one relationship between exit angle and energy implies that the laser acts both as accelerator and spectrometer for free electrons placed near its focus. This property was elegantly exploited by Moore *et al.*, (1995), who determined the energies of electrons released during multiphoton ionization of neon and krypton gas targets by a 1 ps glass laser focused to 10^{18} Wcm^{-2}. As we saw in the previous chapter, barrier suppression creates electrons at well-defined appearance intensities corresponding to successive ionization states. Energy spectra taken within a narrow angular spread should therefore pick up electrons originating from predominantly lower or higher ionization states depending on the viewing angle θ, see Fig. 3.6. As the figure shows, the agreement between the peak angles for given 'release' energies and the theoretical curve is extremely good (see also: Meyerhofer, 1997).

This verification of single electron dynamics was extended to the MeV regime in a slightly more controversial manner by Malka *et al.*, (1997). In

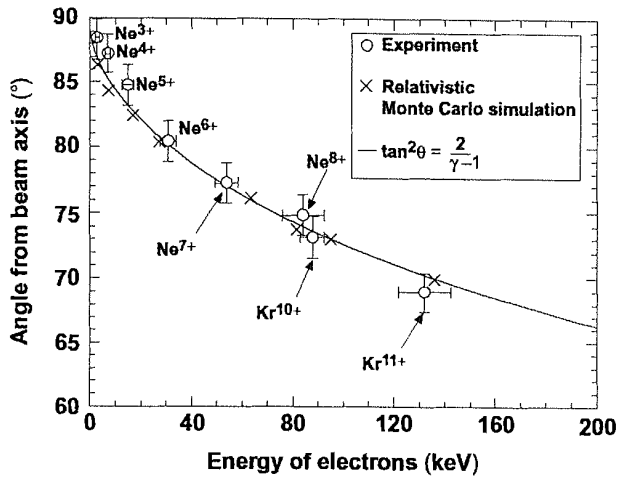

Fig. 3.6 Energies of electrons ejected from a laser focus by the relativistic ponderomotive force. *Courtesy:* D. Meyerhofer, Laboratory for Laser Energetics; Fig. 3 from Meyerhofer (1997). ©IEEE 1997.

their case, the electrons were created by the interaction of a second (ns) laser with a plastic target. These electrons, with energies of a few keV, were then allowed to drift to the center of a target chamber into which the main 500 fs pulse with $I\lambda^2 = 10^{19}$ Wcm$^{-2}\mu$m^2 was focused. Spectra were then measured at two different angles $\theta = 39^o$ and 46^o and compared to a generalized form of Eq. (3.23) (Hartemann *et al.*, 1995):

$$\tan\theta = \frac{\sqrt{2(\frac{\gamma}{\gamma_0} - 1)/(1 + \beta_0)}}{\gamma - \gamma_0(1 - \beta_0)}, \tag{3.24}$$

where $\beta_0 = v_0/c$, the initial drift velocity of the electron before the laser pulse arrives, and $\gamma_0 = (1 - \beta_0^2)^{1/2}$, see also Exercise 4 at the end of the chapter.

To analyze their results, the authors deployed a single-particle model to compute the electron trajectories in the spatially and temporally varying electromagnetic fields of a Gaussian focus, which neglecting phase factors,

look like:

$$E_y = \frac{\sigma_0}{\sigma(x)} E_0 \exp\left\{\frac{-y^2}{\sigma(x)^2}\right\},$$
$$B_z = E_y,$$

where $\sigma(x) = \sigma_0(1+x^2/R_L^2)$ and $R_L = \pi\sigma_0^2/\lambda_L$ is the usual Rayleigh length for a focal spot size σ_0.

Inserting these expressions into the Lorentz equation of motion (3.1) and integrating the orbits for a set of randomly chosen particles near the beam center will lead to final angular spread confined to the xy focal plane. Although this procedure gives agreement with the theoretical prediction Eq. (3.23), it is flawed because the above fields do not satisfy Maxwell's equations! (See Comments provoked by the Malka paper from McDonald (1998) and Mora and Quesnel (1998)). In fact, it is evident that for any focused laser pulse described by a vector potential with radial spatial dependence $A_y = A_0(r)$, there will always be an axial (oscillatory) magnetic field $B_x = \frac{\partial A_y}{\partial z}$. This in turn leads to a force $v_y B_x$ in the z-direction *of the same order* as the y-component of the ponderomotive force (at least for $\sigma_0 \gg \lambda_L$ — see Exercise 3). The net result is that a symmetric, tightly focused laser will tend to eject *rings* of electrons in the forward direction.

3.4 Vacuum Acceleration Schemes

The idea of using lasers to accelerate particles is a compelling one, primarily because of the extremely high electric field strengths $O(10^{12})$ Vm^{-1} which these 'devices' now have to offer. As the simple example in Section 3.1 showed, however, conversion of electromagnetic energy into directed kinetic energy is not that easy. The annoying habit which electrons have of surrendering their energy back to the wave was recognized well before lasers were invented. What is now commonly known as the Lawson-Woodward (LW) theorem (Woodward, 1947; Lawson, 1979) states that an isolated, relativistic electron cannot gain energy by interacting with an EM field. This rather bleak prediction fortunately comes with a number of provisos attached:

(1) the laser field is in vacuum, with no interfering walls or boundaries,
(2) the electron is highly relativistic along the acceleration path,
(3) no static electric or magnetic fields are present,
(4) the interaction region is infinite,

(5) ponderomotive forces are neglected.

It follows that in order to accelerate electrons, one or more of the above conditions must be violated: for example, by focusing the laser to a finite spot size as in Sec. 3.3, which introduces both a radial ponderomotive force *and* limits the interaction region. The introduction of a plasma violates nearly all of the LW assumptions, and a whole host of possibilities open up, which are deferred to Chapters 4 and 7. For now, we concentrate on pure *vacuum* schemes which rely solely on the interaction between a single electron and an electromagnetic wave in various ingenious configurations. A thorough treatment of this subject can be found in the review by Esarey (1995).

Tightly focused, stationary beam

In Sec. 3.3, we saw how a finite focal spot size will cause an electron to drift away from the beam axis, converting its quiver energy into forward-directed kinetic energy in the process. The energy gain from this essentially adiabatic process is roughly the ponderomotive energy: $\Delta U \sim mc^2 a_0^2/4$. This reflects the fact that the electron simply slides down the ponderomotive potential without picking up any longitudinal component: $v_x.E_x = 0$.

A series of studies by Y.K. Ho's group at the Fudan University in Shanghai has shown that this limitation can be overcome, albeit at extremely high intensities ($a_0 > 100$, or $I\lambda^2 > 10^{21}$ $\mathrm{Wcm}^{-2}\mu\mathrm{m}^2$). Wang *et al.*, (2001) show that this process — dubbed 'electron capture' by the authors — works best when the electron is injected *obliquely* into the laser focuses with an incident momentum in the multi-MeV/c range (Kong *et al.*, 2000). Physically, what happens during capture is that the electrons move with the laser phase, thus sampling the field for much longer: the ponderomotive picture (which assumes cycle-averaging) is then no longer applicable. A more recent study by Salamin and Keitel (2002) points out the importance of including higher order terms in the electromagnetic fields in order to correctly describe a tightly (few μm) focused Gaussian beam.

Tailored laser focus

An attractive variation of the above scheme is to confine the electrons to the laser axis by tailoring the radial beam profile so that it creates a ponderomotive potential well. This can be done by clever optics, superimposing higher-order light modes in such a way as to produce an intensity mini-

mum at $r = 0$ (Stupakov and Zolotorev, 2001). Numerical studies of this arrangement predict that extremely high-brightness particle beams might be produced in this fashion.

Sub-cycle acceleration

The most direct way of getting round the LW theorem is to make the laser pulse so short that it comprises only half a cycle, and the electric field does not change sign. This idea may seem fanciful, but technically it is not so far off. Few-cycle pulses (~ 5 fs @ 0.8 μm) are now routinely available, and at increasing intensities, see Chapter 7. Quite a number of schemes have been proposed on sub- or half-cycle pulses. One of the more recent ideas considers crossed beams to create an axial, DC accelerating field capable of producing TeV energy gains for GeV injection energies at 10^{24} Wcm^{-2} (Salamin and Keitel, 2000b).

Other schemes

The number and variety of 'alternative' acceleration schemes is too great to do justice to here, but it is worth mentioning a few of them. The vacuum beat-wave scheme (Esarey *et al.*, 1995; Salamin and Keitel, 2000a) deploys two copropagating laser beams of differing frequencies, beating together to produce a longitudinal axial field via the $\boldsymbol{v} \times \boldsymbol{B}$ force. Highly charged ions can be exploited to overcome the LW theorem by 'holding on' to tightly bound electrons during the laser build up, allowing electrons ionized at the peak amplitude to enjoy phase-matched acceleration during the latter half of the pulse (Hu and Starace, 2002). Finally, static magnetic fields provide a simple way of maintaining the phase-matching condition between electron and fast electrostatic or electromagnetic waves (Katsouleas and Dawson, 1983; Chernikov *et al.*, 1992).

3.5 Relativistic Thomson Scattering

It is a well established fact that accelerated charges act as radiation sources, a property that is exploited to generate x-rays from electrons circulating in a synchrotron, for example. In the present context, it is more appropriate to talk about *scattering* of the incident laser fields. Moreover, the relativistic motion resulting from high laser intensities leads to a high harmonic content in the re-emitted radiation. Thus, free electrons provide an

ideal medium for nonlinear scattering and frequency upshift of high intensity laser pulses, a theme which will recur throughout the chapters which follow. Using the electron orbits $\boldsymbol{r}(t), \boldsymbol{v}(t)$ derived earlier in Sec. 3.1, we can in principle compute the harmonic content of the emitted radiation by substituting these solutions into the standard formulae for light emission by an accelerated charge, discussed extensively in Chapter 14 of Jackson (1975) and which are briefly summarized for convenience here.

The starting point for these formulae are the Liénard-Wiechert potentials, satisfying the wave equations for the scalar and vector radiation potentials caused by a charge in relativistic motion:

$$\phi(\boldsymbol{r},t) = \left[\frac{e}{(1-\boldsymbol{\beta}.\boldsymbol{n})R}\right]_{\rm ret}, \tag{3.25}$$

$$\boldsymbol{A}(\boldsymbol{r},t) = \left[\frac{e\boldsymbol{\beta}}{(1-\boldsymbol{\beta}.\boldsymbol{n})R}\right]_{\rm ret}, \tag{3.26}$$

where $\boldsymbol{\beta} = \boldsymbol{v}/c$, $\boldsymbol{n}$ is a unit vector from the charge in the direction of observation, and the notation $[]_{\rm ret}$ indicates that the argument is to be evaluated at the *retarded* time $t' = t - R(t')/c$, see Fig. 3.7. From Eqs. (3.25 and 3.26), taking special care with the derivatives of retarded quantities, one can obtain the general radiation field seen at point P due to the charge at $\boldsymbol{x}(t)$:

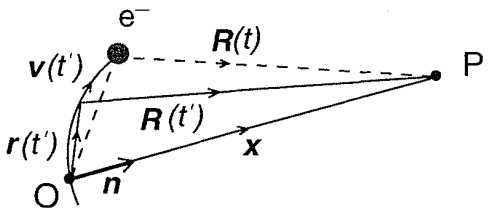

Fig. 3.7 Geometry for calculating radiation fields from a relativistic, accelerated charge.

$$\boldsymbol{E}(\boldsymbol{x},t) = e\left[\frac{\boldsymbol{n}-\boldsymbol{\beta}}{\gamma^2\kappa R^2}\right]_{\rm ret} + \frac{e}{c}\left[\frac{\boldsymbol{n}\times\{(\boldsymbol{n}-\boldsymbol{\beta})\times\dot{\boldsymbol{\beta}}}{\kappa^3 R}\right]_{\rm ret}, \tag{3.27}$$

where $\kappa = dt'/dt = 1 - \boldsymbol{\beta}.\boldsymbol{n}$ and $\dot{\boldsymbol{\beta}} = d\boldsymbol{\beta}/dt$ is the acceleration. Using this field, we can compute the energy flux or Poynting vector at the observation

point P:

$$\boldsymbol{S} = \frac{c}{4\pi}\boldsymbol{E}\times\boldsymbol{B} = \frac{c}{4\pi} \mid E \mid^2 \boldsymbol{n},$$

so that the radiated power per unit solid angle can be written:

$$\frac{dP(t)}{d\Omega} = R^2(\boldsymbol{S}.\boldsymbol{n}) = \frac{c}{4\pi}R^2 \mid E \mid^2 . \tag{3.28}$$

To analyze this further, we assume that the field can be expressed as a Fourier integral:

$$\boldsymbol{E}(t) = \int_{-\infty}^{\infty} e^{-i\omega t}\boldsymbol{E}(\omega)d\omega.$$

Substituting this into Eq. (3.27), and applying Parseval's theorem for power spectra to Eq. (3.28) eventually leads to an *intensity* distribution:

$$\frac{d^2I}{d\omega d\Omega} = \frac{e^2\omega^2}{4\pi^2 c}\left|\int_{-\infty}^{\infty} \boldsymbol{n}\times(\boldsymbol{n}\times\boldsymbol{\beta})e^{i\omega(t-\boldsymbol{n}.\boldsymbol{r}/c)}dt\right|^2 . \tag{3.29}$$

In arriving at this expression the observation point P is assumed to be far away from the charge motion, so that $R(t') \simeq x - \boldsymbol{n}.\boldsymbol{r}(t')$; the additional phase factor $\exp(i\omega x)$ can be ignored. The integral is actually taken over retarded time t' rather than t (primes omitted) and the direction vector $\boldsymbol{n}$ is assumed to be constant in time: hence it is taken along $\overline{OP}$ rather than $\boldsymbol{R}(t')$. Eq. (3.29) gives the energy radiated per solid angle per unit frequency. This is related to the total energy W per solid angle Ω by:

$$\frac{dW}{d\Omega} = \int_{-\infty}^{\infty}\frac{d^2I(\omega,n)}{d\omega d\Omega}d\omega = \int_{-\infty}^{\infty}\frac{dP(t)}{d\Omega}dt. \tag{3.30}$$

One special case of Eq. (3.29) is periodic motion, for which the radiated power P per solid angle Ω can be decomposed into multiples m of the fundamental frequency ω_0, whereby:

$$\begin{aligned}\frac{dP_m}{d\Omega} &= \frac{\omega_0^2}{2\pi}\frac{d^2I_m}{d\omega d\Omega} \\ &= \frac{e^2\omega_0^4 m^2}{(2\pi c)^3}\left|\int_0^{2\pi/\omega_0} \boldsymbol{n}\times(\boldsymbol{n}\times\boldsymbol{v})e^{im\omega_0(t-\boldsymbol{n}.\boldsymbol{r}/c)}dt\right|^2 .\end{aligned} \tag{3.31}$$

We can apply this formula directly to the periodic particle orbits Eq. (3.15) in the average rest frame discussed in Sec. 3.1.2. In the laboratory frame however, the motion is not purely harmonic (as evident from Fig.3.2b), so we have to either go back to Eq. (3.29), or Lorentz-transform

the solution obtained from Eq. (3.31) back from the average rest frame. The latter procedure is quite subtle, and was famously demonstrated by Sarachik and Schappert (1970). The resulting solution for the harmonic power content is intractable for arbitrary polarization and laser amplitude — but see Hartemann (1998). For circularly polarized light, however, a useful form can be found, giving a power spectrum in the average rest frame R:

$$\frac{dP_R^m}{d\Omega_R} = \frac{2m^2A(\omega_R^2)}{\gamma_0^2}\left[\frac{\cot^2\theta_R}{2q^2}J_m^2(\sqrt{2}q\,m\sin\theta) + J'^2_m(\sqrt{2}q\,m\sin\theta_R)\right], \tag{3.32}$$

where

$$A(\omega_R^2) = \frac{e^2\omega_R^2a_0^2}{8\pi c},$$

J_m is the usual Bessel function and J'_m its derivative; θ_R is the angle between the $\boldsymbol{n}$ and the laser wave-vector in the average rest frame (see Fig. 3.8) and $q = a_0/\gamma_0$, $\omega_R = \omega_0/\gamma_0$ corresponding to the orbits on page 34. This formula corresponds to synchrotron radiation from a circulating electron with velocity $\sqrt{2}qc$ at a radius of $\sqrt{2}q/k_R$. This result can be Lorentz-

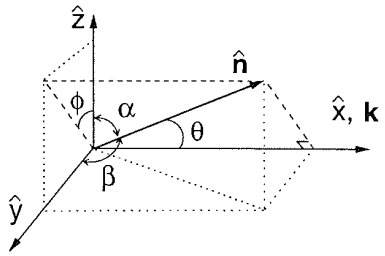

Fig. 3.8 Coordinate system for determining angular dependence of nonlinear Thomson scattering. See Sarachik & Schappert (1970).

transformed back to the lab frame to get the *observed* power spectrum. After proper scaling of angles, time intervals and frequencies, one finally obtains (Sarachik and Schappert, 1970):

$$\frac{dP_L^m}{d\Omega_L} = D(a_0,\theta_L)\frac{dP_R^m}{d\Omega_R}, \tag{3.33}$$

where

$$D(a_0,\theta_L) = \frac{\gamma_0^4}{\left(1+\frac{a_0^2}{2}\sin^2\frac{\theta_L}{2}\right)^4}.$$

The spectrum also no longer consists of integer harmonics of ω_0, but at shifted frequencies given by:

$$\omega_L^m = \frac{m\omega_0}{\left(1+\frac{a_0^2}{2}\sin^2\frac{\theta_L}{2}\right)}. \tag{3.34}$$

In the extreme intensity limit ($a_0 \gg 1$), the radiation is predominantly forward and confined to an angle $\theta_L = \sqrt{8}/a_0$ from the axis of propagation, with a harmonic cutoff at $M = m_{\max} = 3(a_0^2/2)^{3/2}$. This *headlamping* effect is typical of relativistic electrons, and in this case can also be physically understood from the forward drift motion seen earlier. In fact, for circular light, $\theta_L = \theta_p$, the pitch angle of the helical electron orbit given by Eq. (3.10).

For linearly polarized light, the angular distribution is more complex, but follows the qualitative behavior seen with circular light, shifting from sideways to forward due to the increase in drift velocity $v_D \to c$. A more quantitative analysis is possible by expanding the angular radiation pattern Eq. (3.31) for $a_0 < 1$. The total scattered power in the first three harmonics — integrated over solid angle in the laboratory frame — has the following leading terms:

$$\begin{aligned} P_1 &\simeq W_0 \frac{8\pi}{3} a_0^2, \\ P_2 &\simeq W_0 \frac{14\pi}{5} a_0^4, \\ P_3 &\simeq W_0 \frac{621\pi}{224} a_0^6, \end{aligned} \tag{3.35}$$

where $W_0 = e^2\omega_0^2 c/8\pi$ is a characteristic scattered power per electron for a given laser frequency ω_0. The expression for P_1 is readily identified as the classical Thomson scattering result: dividing by the Poynting vector for the incoming light, $S = cE_0^2/8\pi$, yields the Thomson cross-section:

$$\sigma_T = \frac{P_1}{S} = \frac{8\pi}{3}\frac{W_0 a_0^2}{S} = \frac{8\pi}{3} r_0^2,$$

where $r_0 = e^2/mc^2$ is the classical electron radius.

A more thorough discussion of the Sarachik and Schappert work, including an explicit analysis of the angular distribution and some corrections to the higher order coefficients can be found in the article by Castillo-Herrera and Johnston (1993). Other work revisiting this problem by Bardsley *et al.*, (1989) and Mohideen *et al.*, (1992) has reexamined the single electron dynamics, taking into account finite pulse shapes, ionization and space-charge effects. The first two effects mainly give rise to irregularities in the amplitude and phase of the electron orbits which can lead to 'residual heating'; the third effect is potentially the most damaging with regards to harmonic generation in a plasma. As we will see later in Chapter 4, the collective restoring force due to charge separation not only suppresses the drift motion, but produces density nonlinearities which tend to cancel the harmonic-producing relativistic effects.

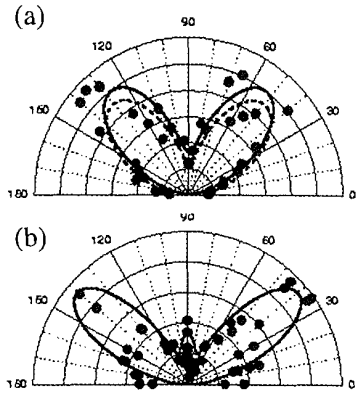

Fig. 3.9 Angular measurements (points) of a) 2nd harmonic light and b) 3rd harmonic light generated by relativistic electrons in a high intensity laser focus. The solid/dashed curves represent theoretically computed radiation patterns. *Courtesy:* D. Umstadter, University of Michigan; Figs. 2 and 3 from Chen *et al.*, (1998b). ©Nature 1998.

Despite the enormous increases in laser intensity seen over the last two decades, experimental evidence for harmonic generation by free electrons has been relatively late in coming. Early observations of 2nd harmonic photons were made by Englert and Rinehart, (1983), but these were at rather low intensities by today's standards. Truly relativistic scattering

has been demonstrated in a landmark paper by Chen, Maksimchuk and Umstadter (1998b), in which angularly resolved measurements of the 2nd and 3rd laser harmonics were shown to qualitatively match the theoretical predictions, thus providing the first unambiguous signature of relativistic figure-of-8 electron motion in a laser field, see Fig. 3.9.

One of the most effective ways of exploiting nonlinear Thomson scattering is to use relativistic electron beams in place of a plasma (Leemans *et al.*, 1997). In this case, the harmonic content is modified by the relative doppler shift of the electron beam (which scales as γ^2), an effect which can be optimized by scattering a short laser pulse off a counterstreaming e-beam (Ride *et al.*, 1995; Hartemann, 1998; He *et al.*, 2003).

3.6 Nonlinear Compton Scattering

Traditionally in electrodynamics, one classifies electron-photon scattering processes according to the recoil energy and momentum acquired by the electron. From the quantum mechanical point of view, this is simply determined by the ratio of the photon energy to the electron rest mass, or $\hbar\omega/mc^2$. For classical Thomson scattering, we have $\hbar\omega/mc^2 \ll 1$, so that recoil effects can be ignored. In Compton scattering one assumes that $\hbar\omega/mc^2 \sim 1$ (or upwards of a few percent), leading to a gain in momentum for the electron, and a corresponding loss of photon energy change, see Fig. 3.10. For single-photon scattering, the energy change ΔE is easily

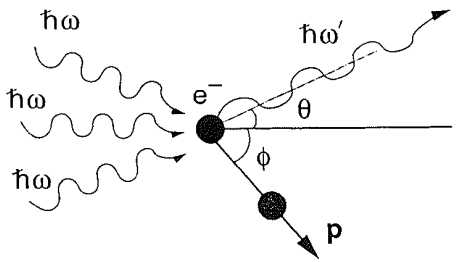

Fig. 3.10 Geometry for multiphoton-electron scattering event in which electron is initially at rest.

found by momentum and energy conservation:

$$\Delta E = \frac{\frac{\hbar\omega}{mc^2}(1-\cos\theta)}{1+\frac{\hbar\omega}{mc^2}(1-\cos\theta)}\hbar\omega, \tag{3.36}$$

which corresponds to the usual wavelength shift of the scattered photon,

$$\Delta\lambda = \lambda' - \lambda = \lambda_c(1-\cos\theta),$$

where $\lambda_c = h/mc = 0.0243$Å is the Compton wavelength.

This situation becomes more complex when the laser intensity — and therefore photon density — becomes high enough to cause *multiphoton* scattering. We have already seen in the previous section that electrons can gain relativistic energies in the 'Thomson regime' if $n\hbar\omega/mc^2 \sim 1$. Moreover, if the electron is *already* relativistic, the photon frequency gets upshifted by γ in the electron rest frame, so that the relevant parameter is $\gamma n\hbar\omega/mc^2$ and the net energy shift takes on a somewhat more complicated form (Meyerhofer, 1997). For a head-on collision ($\theta = 180°$), the maximum backscattered photon energy is:

$$\hbar\omega' = \frac{4n\hbar\omega\gamma^2}{1+\frac{4n\hbar\omega\gamma^2}{mc^2}+a_0^2}.$$

The factor a_0^2 arises from the mass shift or 'dressing' experienced by the electron due to the electromagnetic field. Clearly in this regime, the delineation between nonlinear Thomson and Compton scattering becomes somewhat blurred.

The first experiments to observe multiphoton Compton scattering were performed at the Stanford Linear Accelerator Center (SLAC), where a 47 GeV ($\gamma \simeq 92000$) was 'collided' with a TW, 1 ps, 1 μm laser pulse (Bula *et al.*, 1996). Nd:glass laser photons have an energy of around 1 eV, giving $\gamma\hbar\omega/mc^2 \sim 1$, so that at an intensity of 10^{18} Wcm^{-2}, there is a significant probability of multiple scattering, which scales as $P_n \sim a_0^{2n}$. Sure enough, scattered electrons corresponding to $n = 2, 3$ and 4-photon events were detected in quantities broadly in line with interaction rates predicted by QED theory.

Besides exploring nonlinear QED physics, the photon-e-beam collider configuration (laser/synchrotron) can also be used to generate hard, short pulse x-rays (Leemans *et al.*, 1997), a topic which is examined in Chapter 7. This idea is physically and mathematically very similar to the synchrotron/FEL combination now being pursued at a number of centers

worldwide, reflecting the strong overlap which short pulse laser technology has created between the plasma physics and accelerator communities.

Exercises

(1) The intensity of an electromagnetic (EM) wave with frequency ω is related to its field strength (in cgs units), by $I = cE_0^2/8\pi$.

a) Find the relationship between the normalized pump strength, $a_0 \equiv eE_0/m\omega c$ and the product $I\lambda_L^2$, with I in Wcm^{-2} and λ_L in microns.

b) Determine the transverse oscillation amplitude $x_{\mathrm{osc}} = v_{\mathrm{osc}}/\omega$ of an electron in a beam focused to an intensity of 10^{18} Wcm^{-2} for: i) a Ti:Sapphire laser, ii) a KrF^* laser, iii) a free-electron laser (FEL) with wavelength 1 Å.

(2) The electron orbit in a linearly polarized plane wave $\boldsymbol{A} = a_0 \cos(\omega t - kx)\hat{y}$ is given by:

$$kx = \frac{a_0^2}{4}(\phi + \frac{\sin 2\phi}{2}),$$
$$ky = -a_0 \sin\phi,$$

where $\phi = \omega t - kx$ and a_0 is the normalized field strength as defined in Problem 1.

a) Eliminate ϕ from the first of these equations to demonstrate that when the motion is averaged over a laser cycle, the electron drifts with a velocity

$$v_D = \frac{a_0^2 c}{4 + a_0^2}.$$

b) What are the doppler-shifted frequency and wave vector ω', k' in a reference frame R moving with velocity v_D?

c) Using the result of (b) together with the Lorentz transformations $x' = \gamma_D(x + v_D t), t' = \gamma_D(t + v_D/c^2 x)$, find the electron orbit in R. (Hint: recall that the phase ϕ is Lorentz-invariant). Show that this can

be written in implicit form:

$$16\tilde{x}^2 = \tilde{y}^2(4q^2 - \tilde{y}^2),$$

where $q = a_0/2\gamma_0; \tilde{x} \equiv k'x'; \tilde{y} \equiv k'y'$. Sketch the orbit for i) $a_0 = 0.1$, ii) $a_0 = 1.0$ and iii) $a_0 = 10$. What is the maximum ratio of the transverse:longitudinal oscillations $(y'_{\mathrm{max}}/x'_{\mathrm{max}})$?

(3) The electron in Problem 2 now finds itself in a weakly *in*homogeneous laser field $E_y = E_0(\boldsymbol{r})\sin\phi; B_z = E_0(\boldsymbol{r})/c\sin\phi$, such that the field gradient is small compared to a laser wavelength: $\nabla E_0 \ll E_0/\lambda_L$. The plane wave solution comprises oscillations in x and y about a 'guiding center' moving with velocity v_D.

a) By expanding the fields about the guiding center ($x = v_D t, y = 0$), show that averaged over a laser period, the electron experiences a *ponderomotive force*:

$$\boldsymbol{f}_p = -\frac{e^2}{4\omega^2 m}\nabla E_0^2.$$

(Hint: calculate each component f_{px}, f_{py}, f_{pz} separately).

b) When applied to a plasma fluid, it is usually more appropriate to speak of a *volume* force:

$$\boldsymbol{F}_p = n_e \boldsymbol{f}_p = -\frac{\omega_p^2}{16\pi\omega^2}\nabla E_0^2.$$

Determine the laser intensity at which this ponderomotive force becomes comparable to the thermal plasma pressure $P_e = n_e k_B T_e$.

(4) By including an arbitrary drift v_0 parallel to the laser axis in the energy and momenta conservation relations Eq. (3.21) and Eq. (3.22), show that the ejection angle of an electron is given by Eq. 3.24.

Chapter 4

Laser Propagation in Underdense Plasmas

The physics considered in this chapter is not exclusive to short laser pulses: many of the nonlinear wave phenomena which are confronted here actually predate femtosecond lasers by a good decade or two. Nevertheless, the vast increases in intensity achieved by technological advances — around six orders of magnitude in the last ten years — have ensured that many previously somewhat esoteric ideas, like relativistic self-guiding and plasma-based GeV particle accelerators, are now firmly on the experimental agenda.

Just as with femtosecond laser-solid interactions, which we will meet in the next chapter, much of the 'classical' long pulse theory has to be re-derived because the assumptions about amplitude or timescale are invalid. We will come to many specific examples of this later, but to get a feel for the nature of the processes which occur here, it is perhaps helpful to first look at a few general consequences of high intensity on wave propagation through plasmas. Consider the effect of high field amplitude in a pulse of finite width. Electrons in the plasma see an oscillating electric field $E_0 \sin \omega t$ and according to Eq. (3.7) will acquire a quiver velocity

$$v_0(r,t) = \frac{eE_0(r)}{m\omega_0} \cos \omega t.$$

A laser pulse with a Gaussian radial profile will jiggle the electrons harder at the center than in its wings, resulting in a relativistic 'drag' on the phase fronts in the middle of the beam. In other words, the transverse oscillating current $J \sim n_e v_0(r,t)$, which governs the refractive properties of the medium, has a spatial dependence. This is the physical basis of a number of nonlinear propagation effects, such as self-focusing, filamentation and self-modulation, which all have analogs in other nonlinear media (Shen, 1984). In the present context, the onset of these effects is characterized by